RSC Advances

PAPER

View Article Online
View Journal | View Issue

Cite this: *RSC Adv.*, 2022, **12**, 2810

The effect of particle size and mass ratio on the mechanical response of Al/PTFE/SiC composite with a 2^3 factorial design

Ruiqi Wang, Junyi Huang, Qiang Liu, Shuangzhang Wu, Jiaxiang Wu,* Xinxin Ren and Yuchun Li*

In order to study the effects of different SiC mass ratios, SiC particle sizes and Al particle sizes on the mechanical response of Al/PTFE/SiC, an experiment was conducted through the full 2^3 factorial design. The specimens were prepared by means of molding-vacuum sintering, while the mechanical response of the materials was measured through quasi-static compression. The regression models between failure stress, failure strain and various factors were established respectively and then verified through the analysis of variance (ANOVA) and residual analysis. Besides, the relationship between factors and response as well as that between factors were analyzed using response surface plots. According to the analytical results, the ultimate compressive strength of the material can be improved either by reducing the particle size of SiC and Al or increasing the mass ratio of SiC, while the ductility of the material can be enhanced by maintaining the interaction between SiC mass ratio and SiC particle size at high levels. The interaction effects are significant and can not be ignored, especially the interaction between SiC mass ratio and SiC particle size has an important impact on the mechanical responses, which shows that SiC has a greater influence than Al particles in the material system.

Received 31st October 2021
Accepted 1st January 2022

DOI: 10.1039/d1ra07985a

rsc.li/rsc-advances

1 Introduction

Reactive materials, also known as impact-initiated energetic materials, are designed to release a large amount of energy under highly dynamic load.[1,2] In various military settings, such materials are used to replace those components usually made out of inert materials, such as fragment warheads, shaped charge warheads, penetrating warheads and projectiles. In addition to kinetic energy attack and the physical damage caused to the target, reactive materials can also cause a comprehensive killing effect such as explosion shock, overpressure, and ignition.[3] As for the development of reactive materials, it is in a shift to boosting the strength, density, and reaction energy while limiting the insensitivity of reactive materials.[4]

As a representative reaction material, Al/PTFE has attracted widespread interest from researchers over the past decades, with some significant progress made in formulation, manufacturing and the characteristics of energy release.[5–9] Due to the less desirable mechanical properties and lower density of Al/PTFE than traditional inert projectiles, however, there has now been much attention drawn to improving the mechanical properties of Al/PTFE through addition of different reinforcing particles. With the addition of W particles, as an inert component, PTFE/Al reactive material system can be applied to improve the strength and density of materials. In order to determine the effect of particle size on material density and ultimate compressive strength, Cai *et al.*[10] carried out investigation into the quasi-static and high strain rate mechanical properties of composites consisting of Al, PTFE and W particles by testing the samples with different sizes of W particles. According to the investigative results, the porous composite containing fine W particles has a higher strength than the higher-density material containing coarse W particles. As suggested by Zhang *et al.*,[11] with an increase in the mass ratio of W particles, the properties of Al/PTFE/W materials shifted from being elasto-plastic with significant hardening to being brittle with almost no hardening and the yield stress. In addition, Young's modulus was improved when the mass ratio of W reached a certain level. It was found out by Wang *et al.*[12] that the increase of W mass ratio made no significant difference to the strength of Al/PTFE/W composites, despite the critical failure strain showing an obvious downward trend with the rise in W mass ratio. By comparing the Al/PTFE/W materials shaped by two different treatments, Xu *et al.*[13] obtained the results indicating that under quasi-static compression, the sintered specimens with the same component ratios showed higher failure stress and greater fracture toughness than the pressed Al/PTFE/W reactive material specimens. In recent years, some studies have been conducted with other metals, metal oxides, or metal hydrides introduced into the Al/PTFE system. Integrating Ni

College of Field Engineering, Army Engineering University of PLA, Nanjing, 210007, China. E-mail: wujiaxiang1356@163.com; liyuchunmail@163.com

(nickel) particles into Al/PTFE, Wu *et al.*[14] explored the effect produced by different volume fraction of Ni on the mechanical properties of Al/PTFE/Ni. As suggested by the test results, the existence of Ni was conducive to increasing the strain-hardening modulus and compressive strength of the material. Zhou *et al.*[15] carried out research on the mechanical property of Al/PTFE/CuO(copper oxide), which led to the finding that, the strength of the micro-sized PTFE/Al/CuO first increased and then decreased with an increase in the concentration of Al/CuO thermite. With ZrH_2 introduced into Al/PTFE, Zhang *et al.*[16] drew a conclusion that the gradation of particle size between Al and ZrH_2 produced a more significant effect than particle size.

As a typical ceramic particle, SiC (silicon carbide) has been considered in metal matrix composites, especially in Al/SiC system.[17–21] These achievements suggest the potential of SiC as reinforcing particles to develop the mechanical properties of materials. However, it is rare for prior studies to involve the modification made to Al/PTFE using ceramic particles. With Al/PTFE/SiC granular composites produced by mixing, cold isostatic pressing and vacuum sintering, Wu *et al.*[22] conducted test on its mechanical properties to reach the conclusion that the addition of SiC can enhance the strength of Al/PTFE to a significant extent. Nonetheless, there remains a lack of understanding as to the effects of various factors on the mechanical response of Al/PTFE/SiC reactive materials, such as component ratio and particle size. In addition, the existing approaches to research on the mechanical properties of reactive materials are limited to single factor analysis, and it is difficult to ensure that their response is unaffected by the interaction effect for composites. Therefore, it is necessary to study the impact of various factors on mechanical response of Al/PTFE/SiC through experimentation. Currently, factorial design is widely adopted in experiments, involving several factors. As one of the promising methods used to build the empirical models relating response to factors, it is crucial to study the combined effect of the factors on the response.[23–25]

Based on what has been described above, the 2^3 factorial design was adopted in this study to figure out how the different factors (SiC mass ratios, SiC particle sizes and Al particle sizes) interact with each other and affect the mechanical response of Al/PTFE/SiC reactive materials, such as ultimate compressive strength and failure strain, with an mathematical model connecting factors and responses constructed. The results are expected to provide reference for the formulation optimization, mechanical property enhancement, and engineering applications of Al/PTFE/SiC reactive materials.

2 Experimental

2.1 Factorial design

The 2^3 (three-factor and two-level) factorial design was adopted to analyze the effects of SiC mass ratios and particle size on the mechanical properties of Al/PTFE/SiC under quasi-static compression. SiC mass ratios (A), SiC particle sizes (B), and Al particle sizes (C) were taken as the influencing factors, which varied at two different levels (low and high). Failure stress (S) and failure strain (P) were treated as responses. Given as few as two levels for each factor in a 2^3 factorial design, it was assumed that the responses are approximately linear over the range of the factor levels chosen.[26] The linear hypothesis was satisfied as far as possible by a narrow range of factor levels chosen. Therefore, the mass ratio of SiC was set to 10 wt% (low) and 30 wt% (high) in this experiment, while that of Al and PTFE was fixed at the chemical equilibrium ratio (26%/74%). Additionally, the size of SiC particle was set to 7 μm (low) and 28 μm (high), while that of Al particle was set to 5 μm (low) and 20 μm (high). The factors and responses involved in the design are listed in Table 1.

The model with 3 factors involves 8 different treatment combinations, which were denoted in the standard order as #1, #2, #3, #4, #5, #6, #7, and #8, as shown in Fig. 1. Notably, each corner of the cube corresponds to a set of factor levels, for which each corner corresponds to a treatment combination. For example, #1 represents the treatment combination where factors A, B, and C are all at the low level, while #8 represents the treatment combination where factors A, B, and C are all at the high level. There were five specimens prepared for each treatment combination, so as to reduce the error within treatments, with a total of forty specimens prepared.

The regression model for the full 2^3 factorial design is given as follows:

$$\hat{R} = \beta_0 + \beta_1 x_1 + \beta_2 x_2 + \beta_3 x_3 + \beta_4 x_1 x_2 + \beta_5 x_1 x_3 + \beta_6 x_2 x_3 + \beta_7 x_1 x_2 x_3 \quad (1)$$

where $\hat{R}$ indicates the predicted response, β_0 refers to the intercept, and β_i denotes regression coefficients; x_1, x_2 and x_3 refer to factor coded levels (*i.e.*, +1 and −1); the cross-products x_1x_2, x_1x_3 and x_2x_3 represent the interaction between two factors while $x_1x_2x_3$ indicates the interaction between all factors.

2.2 Material selection and sample preparation

2.2.1 Raw materials. PTFE: 25 μm (from 3 M, Shanghai, China); SiC: 7 μm, 28 μm (from Yinuo, Qinhuangdao, China); Al: 5 μm, 20 μm (from Naiou, Shanghai, China). All specimens were prepared through a process including mixing, cold pressing and sintering, which was based on the patent of Nielson,[27] but the sintering step was slightly different. The preparation process of Al/PTFE/SiC was described as follows: (1) according to the powder proportions and particle sizes of eight treatment combinations in Fig. 1, the original powders of PTFE, Al and SiC were added to an anhydrous ethanol solution, mixed for about 20 minutes through a motor-driven blender, and then dried at 60 °C for 48 hours in a DZG-6050 vacuum dryer (SX, Shanghai, China). (2) Sieve the dry mixture (60 meshers) and then put the powders into a cylindrical mold and cold uniaxial pressed at the pressure of 240 MPa for 20 s to make the cylindrical specimens with the dimension of Φ 10 mm × 10 mm. (3) In light of the sintering process curve in Fig. 2, the molded specimens after cold pressing was sintered in a vacuum sintering furnace at 360 °C for 4 h with the heating rate of 50 °C h^{-1}, which aimed to significantly enhance the mechanical strength.

Table 1 Summary of factors and responses

Factors	Symbols	Unit	Type	Low level (−1)	High level (+1)
SiC mass ratio	*A*	wt%	Numeric	10	30
SiC particle size	*B*	μm	Numeric	7	28
Al particle size	*C*	μm	Numeric	5	20

Responses	Symbols	Unit	Analysis
Failure stress	*S*	MPa	Factorial
Failure strain	*P*		Factorial

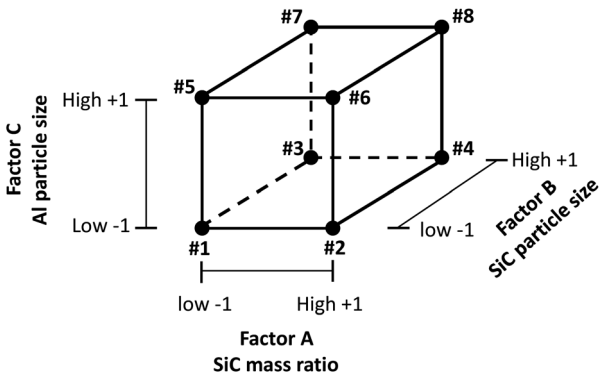

Fig. 1 Geometric view of full 2^3 factorial design.

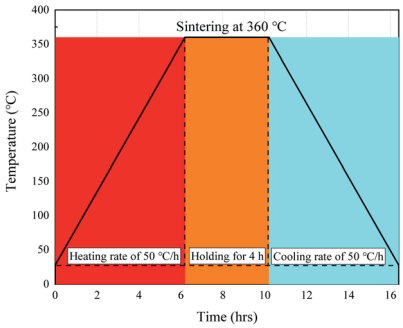

Fig. 2 The sinter temperature curve of reactive materials.

2.3 Experimental procedures

Quasi-static compression tests of the eight types of specimens (40 in total) were conducted by a CMT5105 microcomputer-controlled electronic universal testing machine at 26 °C of the ambient temperature based on the standard GB/T 1041-2008. The load was applied at the speed of 6 mm min^{-1} corresponding to the nominal strain rate of 0.01 s^{-1}. Before the tests, all contact surfaces of the specimens were lubricated with Vaseline to reduce the effect of friction.

Engineering stress and engineering strain could be directly obtained during compression while the true stress and true strain needed to be calculated by the following formulas, which were based on the assumption of constant volume.

$$\begin{cases} \sigma = (1-\varepsilon)\sigma_e \\ \varepsilon = -\ln(1-\varepsilon_e) \end{cases} \quad (2)$$

where σ and ε indicate the true stress and true strain, respectively, σ_e and ε_e refer engineering stress and engineering strain measured by the test machine.

3 Results and discussion

3.1 Quasi-static compression results

Fig. 3 shows the true stress–strain curves of 8 different treatment combinations for Al/PTFE/SiC specimens under quasi

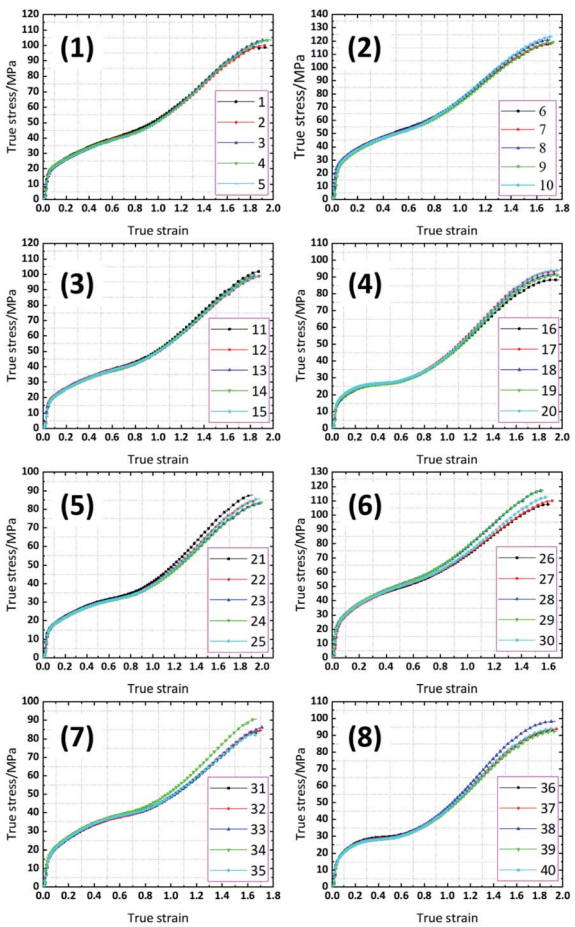

Fig. 3 Stress–strain curves of 8 treatment combinations of Al/PTFE/SiC specimens under quasi static pressure.

Table 2 Full 2^3 factorial design (coded values in bracket) with observed response values

	Factor *A*	Factor *B*	Factor *C*	Response *S*	Response *P*
Treatment	SiC mass ratio (wt%)	SiC particle size (μm)	Al particle size (μm)	Failure stress (MPa)	Failure strain
#1	10 (−1)	7 (−1)	5 (−1)	101.971 ± 1.851	1.952 ± 0.0172
#2	30 (+1)	7 (−1)	5 (−1)	119.756 ± 2.033	1.710 ± 0.0126
#3	10 (−1)	28 (+1)	5 (−1)	99.683 ± 1.128	1.866 ± 0.0215
#4	30 (+1)	28 (+1)	5 (−1)	91.790 ± 1.914	1.956 ± 0.0174
#5	10 (−1)	7 (−1)	20 (+1)	84.966 ± 1.658	1.962 ± 0.0271
#6	30 (+1)	7 (−1)	20 (+1)	112.916 ± 3.816	1.590 ± 0.0303
#7	10 (−1)	28 (+1)	20 (+1)	85.805 ± 2.663	1.698 ± 0.0204
#8	30 (+1)	28 (+1)	20 (+1)	94.405 ± 2.076	1.936 ± 0.0102

static pressure. For example, the curves 1–5 in (1) represent the five repeated experiments on treatment combination #1, while curves 6–10 in (2) represent the five repeated experiments on treatment #2, and so forth. It is worth noting that all specimens were made of elastic–plastic materials despite the treatment specimens showing different response curves. Under quasi-static compression, they first experienced a short linear elastic stage before reaching the yield point. Then, plastic deformation and strain hardening occurred. When the loading stress reached the material failure strength, the specimen was destroyed. Table 2 shows the response values for different treatments, with all measurement results expressed as mean ± standard deviation.

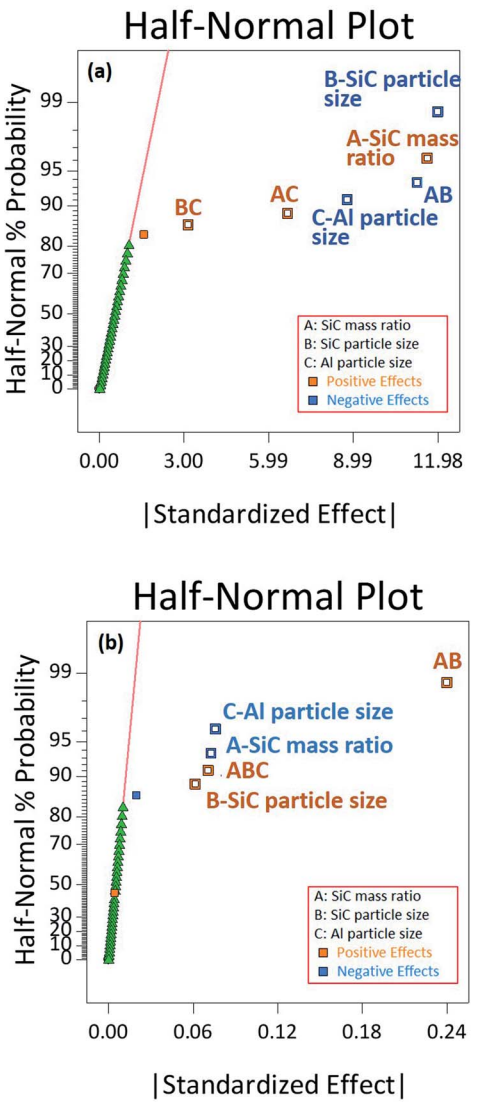

Fig. 4 The half-normal plot of responses (a) *S* and (b) *P*.

3.2 Statistical analysis

3.2.1 Model simplification. Fig. 4 and 5 show the half-normal plot and Pareto chart corresponding to response *S* and response *P* at a 95% confidence, respectively. The use of half-normal plot is purposed to separate the effects into the large and the small to select significant effects and remove insignificant effects to simplify the model. The farther away from the red line, the more significant the effects, and the effects near the red line are insignificant.[28] As shown in the figure, for response *S* (failure stress), the significant effects include *B* (SiC grain size), *A* (SiC mass fraction), *AB* (SiC mass fraction and SiC grain size), *C* (Al grain size), *AC* (SiC mass fraction and Al grain size) and *BC* (SiC grain size and Al grain size); for response *P* (failure strain), the significant effects include *AB*, *C*, *A*, *ABC* and *B*. Pareto chart emphasizes the order of the main and interaction effects that affect models and examines the choice of effects, and the effects above the Bonferroni limit are significant.[29] Thus, with the insignificant items of the model excluded, the simplified model represented by eqn (1) according to the coding parameters is:

$$\hat{S} = +98.91 + 5.81A - 5.99B - 4.39C - 5.63AB + 3.33AC + 1.57BC \quad (3)$$

$$\hat{P} = +1.83 - 0.036A + 0.03B - 0.037C + 0.12AB + 0.035ABC \quad (4)$$

where $\hat{S}$ and $\hat{P}$ are referred as predicted failure stress and predicted failure strain, respectively. *A* is SiC mass ratio; *B* is SiC particle size; *C* is Al particle size.

3.2.2 Variance analysis (ANOVA). As shown in Tables 3 and 4, the significance and adequacy of the regression model after

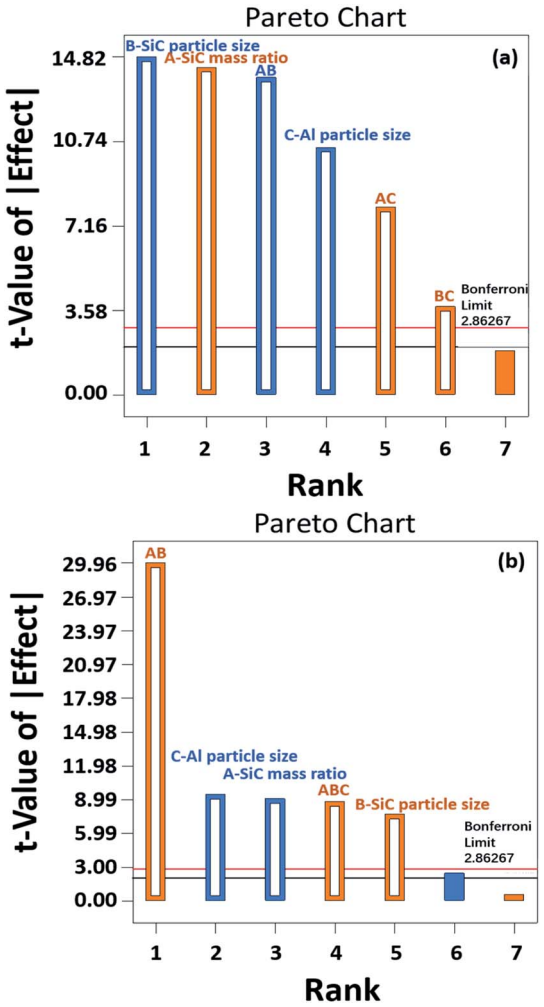

Fig. 5 Pareto chart of responses (a) *S* and (b) *P*.

the exclusion of insignificant coefficients were evaluated by the analysis of variance (ANOVA).[30] The *F*-value of the models is 127.66 for response *S* and is 241.55 for response *P*, indicating that the models are of significance. The values of "Prob > *F*" less than 0.0500 mark model terms are significant. In addition, it can be seen from the tables that all of the selected model items are significant, suggesting the successful simplification of the model and the appropriate adjustment of the model.

R-Squared, also known as the multiple correlation coefficient, is defined as the ratio between the variation caused by the regression and the total variation to express the proximity of the data to the fitted regression line. R-squared is 0.9587 in Table 3 and 0.9726 in Table 4, which means the selected effects can explain 95.87% of the variation in failure stress and 97.26% of the variation in failure strain respectively. Adj *R*-squared and pred *R*-squared are the variants of ordinary *R*-squared that can be used separately to explain the impact made by the number of effects on the model and the accuracy of model prediction response. To achieve "reasonable consistency",[26] adj *R*-squared and pred *R*-squared are supposed to be within about 0.20 of each other. In case of any inconsistence, it is possible for a problem to arise from the data or model. Adj *R*-squared = 0.9512, pred *R*-squared = 0.9393 in Table 3, adj *R*-squared = 0.9686, pred *R*-squared = 0.9621 in Table 4, and the difference between them is less than 0.2. That is to say, the experimental design model is capable of accurately describing the experimental data, suggesting the reliable relationship between effects and responses.

3.2.3 Residual analysis. The residual is referred to as the difference between the experimental and predicted responses, which is assumed to be normally and independently distributed with mean zero and constant variance when the regression equation is constructed.[31] Fig. 6 shows the normal probability plot of external standardized residuals. When the residuals conform to normal distribution, the points on the image will exhibit a linear distribution. It can be seen that the residuals show the general normality. Fig. 7 shows the plot of residuals in comparison with predicted response, which verifies the constancy of variance. Since the points shown in the figure are almost uniformly distributed on both sides of the middle horizontal black line, the residuals meet the variance constant. The two red lines in the figure represent the upper and lower limits of *t* value, while the values outside the red line are referred to as abnormal values. Since all of the data points fall within the range of upper and lower limit *t* values, there is no

Table 3 Summary of ANOVA for response *S*

Source	Sum of squares	Mean square	*F*-Value	*p*-Value prob > *F*	
Model	5364.23	894.04	127.66	<0.0001	Significant
A – SiC mass ratio	1348.03	1348.03	192.49	<0.0001	
B – SiC particle size	1435.53	1435.03	204.98	<0.0001	
C – Al particle size	770.35	770.35	110.00	<0.0001	
AB	1267.21	1267.21	180.95	<0.0001	
AC	444.19	444.19	63.43	<0.0001	
BC	98.93	98.93	14.13	0.0007	
Residual	231.1	7.00			
Cor total	5595.34				
R-Squared	0.9587				
Adj *R*-squared	0.9512				
Pred *R*-squared	0.9393				

Table 4 Summary of ANOVA for response *P*

Source	Sum of squares	Mean square	*F*-Value	*p*-Value prob > *F*	
Model	0.75	0.15	241.55	<0.0001	Significant
A – SiC mass ratio	0.051	0.051	82.75	<0.0001	
B – SiC particle size	0.037	0.037	59.25	<0.0001	
C – Al particle size	0.056	0.056	89.84	<0.0001	
AB	0.55	0.55	897.71	<0.0001	
ABC	0.048	0.048	78.19	<0.0001	
Residual	0.021	6.178×10^{-4}			
Cor total	0.77				
R-Squared	0.9726				
Adj *R*-squared	0.9686				
Pred *R*-squared	0.9621				

abnormality shown by the data. It further evidences that the constructed models perform well in explaining the experimental results.

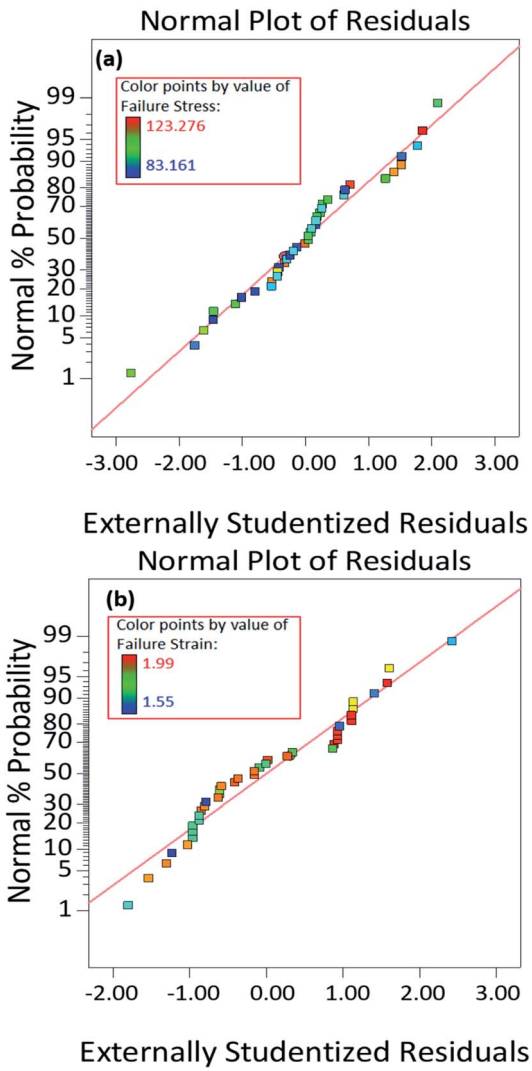

Fig. 6 Normal plot of residuals of responses (a) *S* and (b) *P*.

3.3 Main and interaction effects

3.3.1 Response: *S*. The main effect can be defined as the impact of one factor on the response, with the influence of all other factors ignored. It represents the shift of the response when the factor shifts from low level to high level. As for response *S* (failure stress), *B* (SiC particle size) exerts the most significant influence on failure stress, followed by *A* (SiC mass ratio) and *C* (Al particle size), as revealed by Parto Chart. It is demonstrated that in the Al/PTFE/SiC material system, SiC is the particle with a significant influence and Al is the particle with only insignificant influence on failure stress. For the convenience of expression, SiC is referred to as strong particle and Al is referred to as weak particle. The main effects are illustrated in Fig. 8, where *B* and *C* indicate negative effects while *A* indicates positive effect. In other words, the ultimate compressive strength of the material can be improved either by reducing the particle size of SiC and Al or increasing the mass ratio of SiC. It can also be verified from the treatment combination #2 shown in Table 1 that the failure stress corresponding to the #2 treatment combination is higher compared with all other treatment combinations. When compression occurs, force chains will be formed between fillers, and a smaller the particle size of fillers can increase the strength of force chains, thus significantly improving the strength of materials.[10,11,13,32] When deformation occurs, the interface between the filler and the matrix slides, thus stripping the matrix of the filler. When most of the filler is detached from the matrix, it is unlikely for the stress to be transferred to the filler with strong mechanical properties, thus resulting in the failure of the matrix with weak mechanical properties.

The interaction effect is the effect of one factor on the response as a function of other factors. The resulting model eqn (3) was applied to create three-dimensional plots to demonstrate the aforementioned interaction effects intuitively. Fig. 9–11 show various diagrams of different combinations of significant process parameters for failure stress. All of these graphs were created using color scales to show the changes in response with the modification of factors. The larger the response, the closer the color is to red. Conversely, the smaller the response, and the closer the color is to blue.

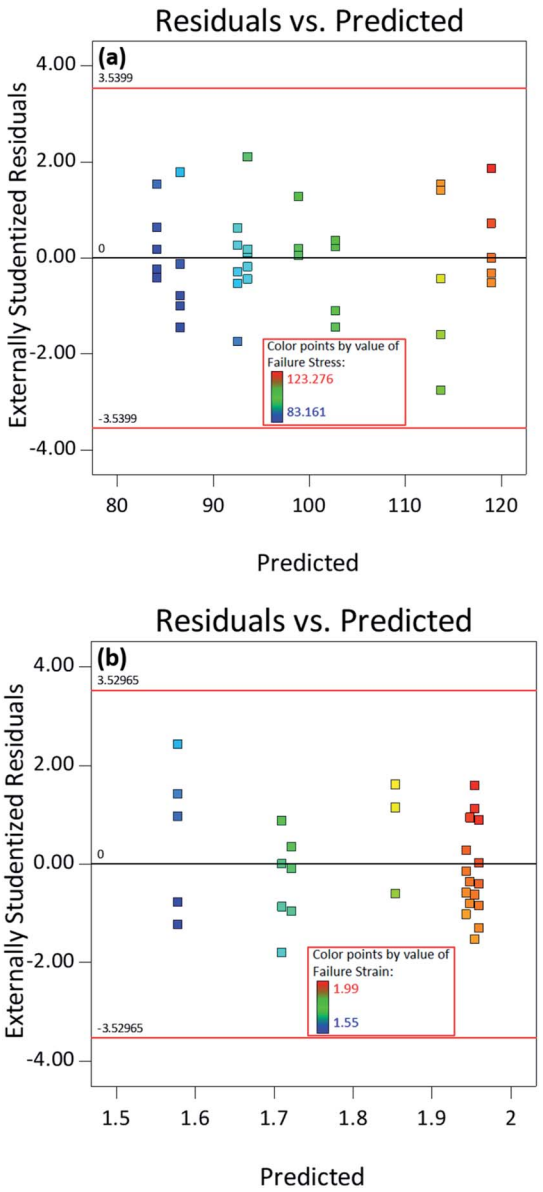

Fig. 7 Plot of residuals *vs.* predicted of response (a) *S* and (b) *P*.

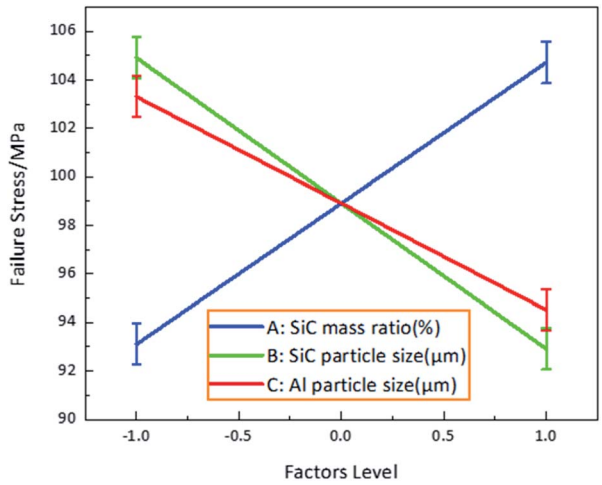

Fig. 8 Main effects of response *S*.

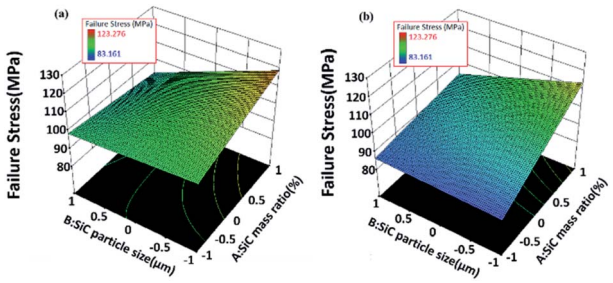

Fig. 9 Response surface plots presenting the dependence of failure stress (*S*) on the SiC mass ratio (*A*) and the SiC particle size (*B*) for the (a) minimum Al particle size ($C = -1$) and (b) maximum Al particle size ($C = 1$).

Fig. 9 shows the impact of SiC mass ratio (*A*) and SiC particle size (*B*) on failure stress (*S*) at a low or high level of Al particle size (*C*). Regardless of level *C*, the impact of *A* on failure stress is made more significant with the decrease of *B*, as is that of *B* with the increase of *A*. That is to say, the impact of SiC mass ratio on failure stress increases with the reduction in SiC particle size. The effect of SiC particle size shows an increasing trend with the rise of SiC mass ratio. When the SiC mass ratio increases to 30% (+1), the SiC particle size decreases to 7 μm (−1), while the failure stress reaches its maximum. Notably, as shown in (Fig. 9(a)), the failure stress increases with the rise of *A* when *B* stays low. When *B* is at high levels, the failure stress declines with the increase of *A*. According to (Fig. 9(b)), however, the failure stress shows an upward trend with the increase of *A*, which is irrelevant to the level of *B*. It means that the continued addition of strong particles will reduce the compressive strength of the material when the strong particles (SiC) have a large particle size and the gradation of particle size does not match. When the weak particles (Al) have a large size, the continued addition of strong particles will remain effective in improving the strength of the material even if the gradation of particle size does not match.

Fig. 10 shows how the SiC mass ratio (*A*) and Al particle size (*C*) impact on failure stress (*S*) at a low or high level of SiC

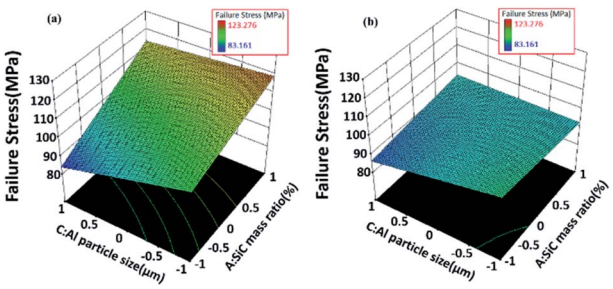

Fig. 10 Response surface plots presenting the dependence of failure stress (*S*) on the SiC mass ratio (*A*) and the Al particle size (*C*) for the (a) minimum SiC particle size ($B = -1$) and (b) maximum SiC particle size ($B = 1$).

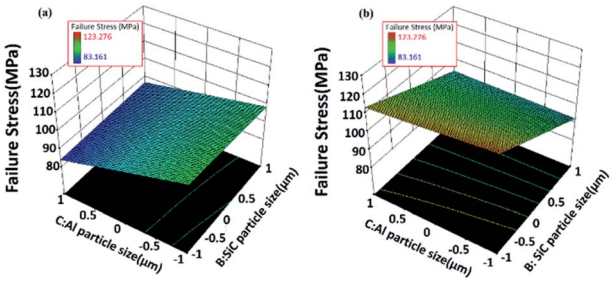

Fig. 11 Response surface plots presenting the dependence of failure stress (S) on the SiC particle size (B) and the Al particle size (C) for the (a) minimum SiC mass ratio ($A = -1$) and (b) maximum SiC mass ratio ($A = 1$).

particle size (B). When B is at a low level as shown in (Fig. 10(a)), the impact of C on failure stress increases with the decrease of A, while the effect of A is basically unaffected by C. In other words, the effect of Al particle size on failure stress is enhanced with the decrease of SiC mass ratio. The impact of SiC mass ratio on response is unaffected by the particle size of Al. When B is at a high level as shown in (Fig. 10(b)), there is barely any interaction occurring between A and C, suggesting that the effect of SiC mass fraction on failure stress is more significant than that of Al particle size. Especially when SiC has a small particle size, the greater the SiC mass fraction, the greater the failure stress.

Fig. 11 shows how the SiC particle size (B) and Al particle size (C) impact on failure stress (S) at a low or high level of SiC mass ratio (A). When A is at a low level as shown in (Fig. 11(a)), the impact of C on response is more significant than that of B. With the decline in C, the failure stress of the material rises. When A is at a high level, the impact of B is more significant than that of C. As B decreases, the level of material failure stress increases. It is suggested by the results that even strong particles have a less significant effect on compressive strength than weak particles at a lower mass ratio.

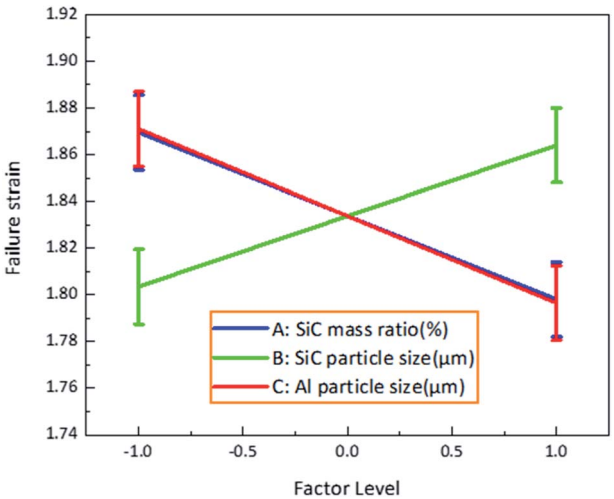

Fig. 12 Main effects of response P.

3.3.2 Response: *P*. With regard to response P (failure strain), the main effects are shown in Fig. 12, which reveals that C and A have negative effects while B has a positive effect. That is to say, the ductility of the material can be reduced by increasing the Al particle size and SiC mass ratio, while it can be improved by increasing the SiC particle size. From Table 1, however, it can be found out that when the treatment is A (−1), B (+1) and C (−1) (corresponding to the treatment combination #2 in Table 1), the failure strain does not reach the maximum, while the failure strain is relatively high for #1, #4, #5 and #8. Fig. 13 shows the top view of these groups of specimens. Apparently, #2 specimens have a lower ductility than other groups of specimens after compression, which is because the impact of interaction overwhelms the main effects, as can be observed in the Pareto chart. The commonality between #1, #4, #5 and #8 treatment combinations is that their AB interaction stays at a high level.

Although ABC interaction is also play a significant role in failure strain, usually, the third-order interaction is not insignificant in many cases. If it is of significance, this may be attributed to the strong interference from the second-order interaction, which is known as effect inheritance.[26] For interaction ABC, the corresponding second-order interactions are AB, BC and AC, of which BC and AC are far less significant than the impact of ABC interaction, AB is far more significant than the impact of ABC interaction, while both ABC and AB exert positive effects. On this basis, it can be concluded that the significance of ABC is attributed to the significant impact of AB interaction. Similarly, the response surfaces plot of AB interaction effect was described using the model eqn (4), as shown in Fig. 14. It shows the impact of SiC mass ratio (A) and SiC particle size (B) on failure strain (P) at a low or high level of Al particle size (C). The response surface exhibits a large curvature, which suggests the significant interaction effect between A and B.

It is noteworthy that the relationship between A and P shows direct proportionality when the SiC particle size is at the higher level ($B > 0$), and that A is inversely proportional to P when B is at a lower level ($B < 0$). Therefore, the failure strain can reach its maximum only when A and B reach the maximum or minimum simultaneously.

Through comparison with (Fig. 14(a) and (b)), it can be discovered that there is no visible change in the areas with high AB interaction effect. That is to say, the materials with 10% SiC (7 μm) and 30% SiC (28 μm) are barely affected by Al particle size, while the materials with low AB interaction effect decrease significantly with the change in Al particle size. It is also suggested

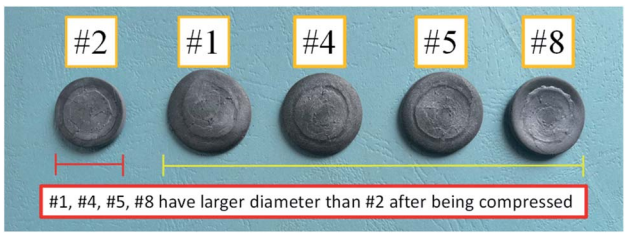

Fig. 13 Top view of specimens after compression.

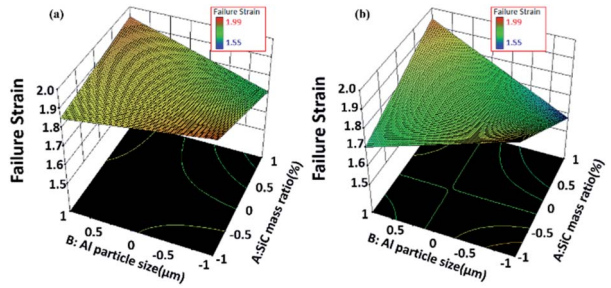

Fig. 14 Response surface plots presenting the dependence of failure strain (P) on the SiC mass ratio (A) and the SiC particle size (B) for the (a) minimum Al particle size ($C = -1$) and (b) maximum Al particle size ($C = 1$).

that the AB interaction effect is more significant than C although the main factors A (SiC mass ratio) and B (SiC particle size) have a less significant impact on the response P (failure strain) than C (Al particle size), which means SiC remains the particle with a strong influence on the response of failure strain.

4 Conclusions

In this paper, an in-depth study was conducted on how the selected factors (SiC mass ratio; SiC particle size; Al particle size) would affect the mechanical response (failure stress and failure strain) of Al/PTFE/SiC. The regression equations between responses and factors under quasi-static pressure was obtained through a full 2^3 factorial design. The accuracy and applicability of the model were verified through the analysis of variance and residual analysis. Besides, the response surface plots were drawn to analyze the relationship between each factor and responses. The conclusions reached in this study are presented as follows:

(1) As for the failure stress, the order of impact made by the main factors is: SiC particle size > SiC mass ratio > Al particle size. The ultimate compressive strength of the material can be improved either by reducing the particle size of SiC and Al or increasing the mass ratio of SiC.

(2) Regarding the failure strain, the impact of interaction between SiC mass ratio and SiC particle size exceeds the main effects. When the SiC mass ratio and SiC particle size reach the high level or low level simultaneously, the ductility of the material can be improved.

(3) The interaction between SiC mass ratio and SiC particle size plays a vitally important role in both mechanical responses. Therefore, SiC is the particle with a strong influence and Al is the particle a weak influence in the Al/PTFE/SiC material system.

Conflicts of interest

The authors declare that there is no conflict of interest regarding the publication of this paper.

Acknowledgements

The financial support from the National Natural Science Foundation of China (General Program, Grant No. 51673213) is gratefully acknowledged.

Notes and references

1 F. Y. Xu, B. Q. Geng, X. P. Zhang, *et al.*, Experimental study on behind-plate overpressure effect by reactive material projectile, *Propellants, Explos., Pyrotech.*, 2016, **42**, 192–197.
2 H. F. Wang, H. Guo, B. Geng, *et al.*, Application of PTFE/Al Reactive Materials for Double-Layered Liner Shaped Charge, *Materials*, 2019, **12**, 2768.
3 M. Wei, Damage Effects of Energetic Fragment Warhead, *Chin. J. Energ. Mater.*, 2011, **19**(4), 450–453.
4 E. M. Hunt, *et al.*, Impact ignition of nano and micron composite energetic materials, *Int. J. Impact Eng.*, 2009, **36**, 842–846.
5 H. F. Wang, B. Q. Geng, *et al.*, The effect of sintering and cooling process on geometry distortion and mechanical properties transition of PTFE/Al reactive materials, *Def. Technol.*, 2020, **16**, 720–730.
6 F. Y. Xu, Y. F. Zheng, *et al.*, Experimental study on penetration behavior of reactive material projectile impacting aluminum plate, *Int. J. Impact Eng.*, 2016, **95**, 125–132.
7 X. Q. Xiang, W. H. Xiao and Q. Lei, Study on the Impacting Thermal Effects of PTFE/Al Energetic Materials, *DEStech Transactions on Engineering and Technology Research*, 2017, 1–6.
8 B. Feng, X. Fang, H. X. Wang, *et al.*, The Effect of Crystallinity on Compressive Properties of Al-PTFE, *Polymers*, 2016, **8**(10), 356.
9 H. F. Wang, Y. F. Zheng, Q. Yu, *et al.*, Impact-induced initiation and energy release behavior of reactive materials, *J. Appl. Phys.*, 2011, **110**(7), 239–245.
10 J. Cai, F. Jiang and K. S. Vecchio, Mechanical and microstructural properties of PTFE/Al/W system, *AIP Conf. Proc.*, 2007, **955**, 723.
11 X. F. Zhang, J. Zhang, L. Qiao, *et al.*, Experimental study of the compression properties of Al/W/PTFE granular composites under elevated strain rates, *Mater. Sci. Eng., A*, 2013, **581**, 48–55.
12 L. Wang, J. Liu, S. Li, *et al.*, Investigation on reaction energy, mechanical behavior and impact insensitivity of W-PTFE-Al composites with different W percentage, *Mater. Des.*, 2016, **92**, 397–404.
13 F. Y. Xu, S. B. Liu, Y. F. Zheng, *et al.*, Quasi-Static Compression Properties and Failure of PTFE/Al/W Reactive Materials: Quasi-Static Compression Properties, *Adv. Eng. Mater.*, 2016, **19**(1), 1600350.
14 J. X. Wu, H. X. Wang, X. Fang, *et al.*, Investigation on the Thermal Behavior, Mechanical Properties and Reaction Characteristics of Al-PTFE Composites Enhanced by Ni Particle, *Materials*, 2018, **11**(9), 1741.
15 J. Zhou, L. Ding, W. Tang, *et al.*, Experimental Study of Mechanical Properties and Impact-Induced Reaction Characteristics of PTFE/Al/CuO Reactive Materials, *Materials*, 2020, **13**(1), 66.
16 J. Zhang, Y. C. Li, J. Y. Huang, *et al.*, The effect of al particle size on thermal decomposition, mechanical strength and

sensitivity of Al/ZrH_2/PTFE composite, *Def. Technol.*, 2021, **17**, 829–835.

17 M. Shaikh, T. Aziz, S. Arif, *et al.*, Effect of sintering techniques on microstructural, mechanical and tribological properties of Al-SiC composites, *Surf. Interfaces*, 2020, **20**, 100598.

18 A. F. Meselhy and M. M. Reda, Investigation of mechanical properties of nanostructured Al-SiC composite manufactured by accumulative roll bonding, *J. Compos. Mater.*, 2019, **53**, 3951–3961.

19 S. Huo, L. Xie, J. Xiang, *et al.*, Atomic-level study on mechanical properties and strengthening mechanisms of Al/SiC nano-composites, *Appl. Phys. A: Solids Surf.*, 2018, **124**, 1–12.

20 S. Sulaiman, Z. Marjom, M. Ismail, *et al.*, Effect of Modifier on Mechanical Properties of Aluminium Silicon Carbide (Al-SiC) Composites, *Procedia Eng.*, 2017, **184**, 773–777.

21 P. R. Matli, U. Fareeha, R. A. Shakoor, *et al.*, Fabrication and Mechanical Properties of Extruded Al-SiC Nanocomposites, *Nano Hybrids and Composites*, 2017, **16**, 12–19.

22 J. X. Wu, J. Y. Huang, Q. Liu, *et al.*, Influence of ceramic particles as additive on the mechanical response and reactive properties of Al/PTFE reactive composites, *RSC Adv.*, 2020, **10**, 1447–1455.

23 C. Cai, H. Zhang, X. Zhong, *et al.*, Ultrasound enhanced heterogeneous activation of peroxymonosulfate by a bimetallic Fe–Co/SBA-15 catalyst for the degradation of Orange II in water, *J. Hazard. Mater.*, 2015, **283**, 70–79.

24 M. Edrissi and R. Norouzbeigi, Synthesis of deer horn-like and spherical ZnO nanoparticles by microwave decomposition of bis(2-pyridinethiol N -oxide)zinc using factorial and Taguchi experimental designs, *J. Mater. Sci.: Mater. Electron.*, 2011, **22**(4), 328–334.

25 V. N. Gaitonde, S. R. Karnik, J. C. Rubio, *et al.*, Analysis of parametric influence on delamination in high-speed drilling of carbon fiber reinforced plastic composites, *J. Mater. Process. Technol.*, 2008, **203**(1–3), 431–438.

26 D. C. Montgomery *Design and Analysis of Experiments*, 8th edn, 2012.

27 G. Lund, D. Nielson and R. Tanner, High strength reactive materials, *US Pat.*, 20030096897, 2003.

28 N. Balakrishnan, T. Colton, B. Everitt, *et al.*, *Wiley StatsRef: Statistics Reference Online ‖ Half-Normal Plots*, 2014.

29 P. Kiesow, The Pareto chart–a tool for continuous improvement, *Ceram. Ind.*, 1995, **144**, 20.

30 M. G. Larson, Analysis of variance, *Circulation*, 2008, **117**(1), 115–121.

31 J. S. Nobre and J. M. Singer, Residual Analysis for Linear Mixed Models, *Biom. J.*, 2010, **49**, 5.

32 E. B. Herbold, V. F. Nesterenko, D. J. Benson, *et al.*, Particle size effect on strength, failure and shock behavior in Polytetrafluoroethylene-Al-W granular composites, *J. Appl. Phys.*, 2008, **104**, 1007.